

# Editors' Choice—Perspective—Challenges in Moving to Multiscale Battery Models: Where Electrochemistry Meets and Demands More from Math

Krishna Shah,<sup>1,\*</sup><sup>®</sup> Akshay Subramaniam,<sup>2,\*</sup><sup>®</sup> Lubhani Mishra,<sup>1</sup><sup>®</sup> Taejin Jang,<sup>1,\*</sup><sup>®</sup> Martin Z. Bazant,<sup>3,\*\*</sup> Richard D. Braatz,<sup>3,\*\*</sup> and Venkat R. Subramanian<sup>1,\*\*\*,z</sup><sup>®</sup>

<sup>1</sup>UT, Austin, Texas 78712, United States of America
 <sup>2</sup>UW, Seattle, Washington 98195, United States of America
 <sup>3</sup>MIT, Cambridge, Massachusetts 02139, United States of America

There has been significant recent interest in studying multiscale characteristics of current and next-generation batteries, including lithium-metal and lithium-sulfur batteries. Advances in computing power make researchers believe that the detailed multiscale models can be efficiently simulated to arrive at the insights for the degradation and performance loss; however, this is not true and special attention needs to be paid to local singularities, boundary layers, moving boundaries, etc. This article presents 2D examples that illustrate the importance of grid convergence studies, provides well-defined detailed models to test the efficiency of numerical schemes, and discusses the associated simulation challenges.

© 2020 The Author(s). Published on behalf of The Electrochemical Society by IOP Publishing Limited. This is an open access article distributed under the terms of the Creative Commons Attribution Non-Commercial No Derivatives 4.0 License (CC BY-NC-ND, http://creativecommons.org/licenses/by-nc-nd/4.0/), which permits non-commercial reuse, distribution, and reproduction in any medium, provided the original work is not changed in any way and is properly cited. For permission for commercial reuse, please email: permissions@ioppublishing.org. [DOI: 10.1149/1945-7111/abb37b]

Manuscript submitted June 11, 2020; revised manuscript received August 20, 2020. Published September 24, 2020. Models 1 and 2 in this article were presented during the invited talk# F04-1128 at the Dallas, Texas, Meeting of the Society, May 26–May 30, 2019.

Though porous electrode pseudo-two-dimensional (p2D) models have been the standard for the study, analysis, and design (and recently control) of lithium-ion batteries, the second dimension (parallel to the current collector) is becoming important for the next-generation batteries.<sup>1</sup> This is particularly true when studying uneven lithium metal deposition on the anode surface in a lithium metal battery, which leads to dendrite formation.<sup>2,3</sup> Many numerical methods have been used to simulate multiscale battery models, including finite difference, finite volume, finite element, phase-field, and level-set methods. A typical assumption is that a brute force approach with a large number of nodes/ elements will help resolve the physics to an acceptable accuracy. In this work, we provide detailed models, discuss numerical challenges in their simulation, and share our perspective on relevant numerical details.

#### **Current Status**

Motivating examples—two-dimensional steady-state currentpotential distribution—For demonstration purposes, two simple steady-state problems are considered, one with primary current distribution (PCD) and the other with secondary current distribution (SCD). A two-dimensional square domain ( $L_x = L_y$ ) is considered for both problems. The partial differential equation (PDE) and required boundary conditions for these two problems are given in Models 1 and 2.

Model 1

$$\frac{\partial}{\partial X} \left( \frac{\partial \phi}{\partial X} \right) + \frac{\partial}{\partial Y} \left( \frac{\partial \phi}{\partial Y} \right) = 0$$
  
$$\frac{\partial \phi}{\partial X} = 0 \quad \text{at } X = 0, 1$$
  
$$\phi = 0 \quad \text{at } Y = 1$$
  
$$\phi = 1 \quad \text{at } Y = 0, 0 \leqslant X \leqslant 0.5$$
  
$$\frac{\partial \phi}{\partial Y} = 0 \quad \text{at } Y = 0, 0.5 < X \leqslant 1$$
[1]

Model 2

$$\frac{\partial}{\partial X} \left( \frac{\partial \phi}{\partial X} \right) + \frac{\partial}{\partial Y} \left( \frac{\partial \phi}{\partial Y} \right) = 0$$
  
$$\frac{\partial \phi}{\partial X} = 0 \quad \text{at } X = 0, 1$$
  
$$\phi = 0 \quad \text{at } Y = 1$$
  
$$\frac{\partial \phi}{\partial Y} = \phi - 1 \quad \text{at } Y = 0, 0 \leq X \leq 0.5$$
  
$$\frac{\partial \phi}{\partial Y} = 0 \quad \text{at } Y = 0, 0.5 < X \leq 1$$
  
[2]

*Models* 1 *and* 2 are limited to finding the ohmic drop across the separator domain in the absence of concentration gradients. Mass transfer-limited current distribution at steady state for binary electrolyte also results in Laplace's equation.<sup>4–7</sup>

These models consider PCD or SCD at Y = 0,  $0 \le X \le 0.5$ , indicating that only a part of the separator is in contact with the anode. This singularity at X = 0.5, Y = 0, which is the anode/insulator interface, is a key aspect in simulating lithium metal batteries. The Dirichlet condition is applied at Y = 1, which can be viewed as the bulk condition or setting the cathode potential to a particular value. The rest of the sides of the domain are treated as walls with zero flux.

*Numerical method—FEM*—The Finite Element Method (FEM) is a widely used discretization method for 2D models.

The underlying mathematical formulation consists of the weak form being applied to each element:

$$\begin{split} &\int_{y=-b}^{y=b} \int_{x=-a}^{x=a} \frac{\partial W}{\partial x} \frac{\partial \phi}{\partial x} dx dy + \int_{y=-b}^{y=b} \int_{x=-a}^{x=a} \frac{\partial W}{\partial y} \frac{\partial \phi}{\partial y} dx dy \\ &= \int_{\Gamma} W \bigg( \frac{\partial \phi}{\partial x} n_x + \frac{\partial \phi}{\partial y} n_y \bigg) dx dy \end{split}$$
[3]

where

$$\phi = \sum_{i=1}^{m} N_i \phi_i$$
[4]

\*\*Electrochemical Society Member.

\*\*\*Electrochemical Society Fellow.

<sup>z</sup>E-mail: venkat.subramanian@utexas.edu

and the weight function is taken to be  $W = \phi$  and N<sub>i</sub> are the shape functions. Bilinear shape functions are given by



<sup>\*</sup>Electrochemical Society Student Member.

$$N_{1} = \frac{1}{4} \left( 1 - \frac{x}{a} \right) \left( 1 - \frac{y}{b} \right); \quad N_{2} = \frac{1}{4} \left( 1 + \frac{x}{a} \right) \left( 1 - \frac{y}{b} \right)$$
$$N_{3} = \frac{1}{4} \left( 1 + \frac{x}{a} \right) \left( 1 + \frac{y}{b} \right); \quad N_{4} = \frac{1}{4} \left( 1 - \frac{x}{a} \right) \left( 1 + \frac{y}{b} \right)$$
[5]

where a and b are half of the element sizes in the x and y directions, respectively. This formulation is applied to each element resulting in the linear matrix equation

$$A\Phi = B$$
 [6]

where  $\Phi$  is a vector containing the discretized values of  $\phi$  to be solved at each node in the domain.

Some of the different types of shape functions that can be used are bilinear, biquadratic, and bicubic. The choice of the shape function greatly affects the order of convergence and the number of equations to be solved for a given number of elements. The coefficient matrix A in Eq. 6 is sparse, and linear solvers which exploit sparsity are typically used for efficiency. Both *Models 1* and 2 are solved using in-house FEM codes validated with COMSOL Multiphysics 5.4.

*Error analysis*—*PCD*—There are different approaches to quantify the numerical accuracy and convergence of the FEM.<sup>8</sup> When this problem was first attempted with in-house FEM codes, and later confirmed with COMSOL Multiphysics 5.4, the obtained results seemed to oscillate for the 4<sup>th</sup> or 5<sup>th</sup> digit after the decimal. Having a very fine mesh near the singularity helps in recovering the expected order of convergence away from the singularity. However, our interest lies in the values of the variables at the electrode surface where the singularity exists. A simple error analysis is performed by comparing the numerical solutions with the analytical solution obtained using conformal mapping technique.<sup>9,10</sup> Results are given in Table I. Observations from Table I are

• All the three shape functions provide only first-order convergence, with bilinear shape functions having the advantage of lowest cost. For robust simulations, smaller element size and bilinear shape functions can be used near singularities, and higher order methods with larger element size elsewhere.<sup>11</sup>

• Because of strong singularity, FEM solution converged only to 1 digit after the decimal for the average current density, leading to poor prediction of the ohmic resistance.

Similar conclusions are expected from any numerical method unless mesh adaptivity is used. Fortunately, the error in battery models may be less for SCD, which is analyzed next.

*Error analysis*—*SCD*—In this case, the exact solution is not available, and the error analysis is performed by comparing the values by doubling the number of elements in both x and y directions. Results are summarized in Table II. Observations from Table II are

• Unlike the PCD, the SCD benefited from higher order methods. When high numerical accuracy is desired ( $E_r \le 1E-8$ ), bicubic shape functions are found to be marginally better than the biquadratic shape functions.

• FEM solution converged very quickly to 6 to 8 digits after the decimal, but convergence was sluggish after that.

• As expected, the numerical accuracy is lower near the singular point.

An approximate analytical solution in the form of an infinite series can be written as

$$\phi = A_0(1 - Y) + \sum_{i=1}^{n} A_i \cos(i\pi X) \sinh(i\pi(1 - Y))$$
 [7]

where the coefficients are calculated using the boundary condition at Y = 0,

$$\begin{split} \int_{X=0}^{X=1/2} \left( \frac{\partial \phi}{\partial Y} \Big|_{Y=0} - (\phi(X, 0) - 1) \right) \cos(j\pi X) dX \\ + \int_{X=1/2}^{X=1} \frac{\partial \phi}{\partial Y} \Big|_{Y=0} & \cos(j\pi X) dX = 0 \end{split}$$
[8]

where j varies from 0 to n. This series solution converges to 6, 8, and 12 digits of accuracy with 5, 10, and 5000 terms, respectively (for  $\phi$  at the anode).

These models become more complicated when additional physical phenomena are considered. Some of them are summarized in the subsequent sections.

*Modifying the model for lithium metal battery architecture*— Under the same assumption of absence of concentration gradients, the steady-state model for the potential in the separator region with Butler–Volmer (BV) kinetics is given in *Model 3* 

Model 3

$$\begin{pmatrix} \frac{L_{y}^{2}}{L_{x}^{2}} \end{pmatrix} \frac{\partial^{2} \phi}{\partial X^{2}} + \frac{\partial^{2} \phi}{\partial Y^{2}} = 0 \frac{\partial \phi}{\partial X} = 0 \text{ at } X = 0, 1 \phi = 0 \text{ at } Y = 1 - \frac{\partial \phi}{\partial Y} = 2i_{0, \text{scaled}} \sinh\left(\frac{\eta}{2}\right) \\ \eta = V_{\text{anode}} - \phi = 1 - \phi \end{cases} \text{ at } Y = 0, 0 \leqslant X \leqslant 0.5 \eta = V_{\text{anode}} - \phi = 1 - \phi \end{cases} \text{ at } Y = 0, 0.5 < X \leqslant 1 i_{0, \text{scaled}} = \frac{i_{0}L_{y}F}{\kappa RT}$$
 [9]

where the ratio of  $L_y$  and  $L_x$  is the aspect ratio, and  $V_{anode}$  denotes the voltage of the anode which is specified to a fixed value,  $V_{anode} = 1$ .

FEM is applicable here, with the nonlinearity in the boundary condition at the anode being addressed using a Newton–Raphson (NR)-type iteration scheme. Typically, NR is iterated to much looser tolerance compared to machine precision (1E-8 or 1E-10, for example). It should be noted that the error introduced by a NR-type solver is in addition to the discretization error.

*Time dynamics*—The Laplace's equation can provide the potential distribution in the separator region only in the absence of concentration gradients, and when there is a quasi-steady state.

Variable of Interest	Element Size $h_x = h_y$ = h	Bilinear			Biquadratic			Bicubic		
		Numerical Solution	$\begin{array}{l} & Error \\ E_a = \\  Numerical \\ solution \\ -Analytical \\ solution^{a)}  \end{array}$	Order of Convergence $\log_2\left(\frac{E_a(h)}{E_a(h/2)}\right)$	Numerical Solution	$\begin{array}{l} & Error \\ E_a = \\  Numerical \\ solution \\ -Analytical \\ solution^{a)}  \end{array}$	Order of Convergence $\log_2\left(\frac{E_a(h)}{E_a(h/2)}\right)$	Numerical Solution	$\begin{array}{l} & Error \\ E_a = \\  Numerical \\ solution \\ -Analytical \\ solution^{a)}  \end{array}$	Order of Convergence $\log_2\left(\frac{E_a(h)}{E_a(h/2)}\right)$
$\frac{\partial \phi}{\partial \mathbf{Y}}(0, 0)$	1/100	-1.1594	1.87896E-03	1.0351	-1.16076	5.51613E04	0.9698	-1.16102	2.92713E-04	1.0000
	1/200	-1.1604	9.16912E-04	1.0181	-1.16103	2.81638E-04	0.9851	-1.16117	1.46358E-04	1.0000
	1/400	-1.1609	4.52738E-04	1.0092	-1.16117	1.42284E-04	0.9925	-1.16124	7.31788E-05	1.0000
	1/800	-1.1611	2.24930E-04	1.0046	-1.16124	7.15124E-05	0.9964	-1.16127	3.65899E-05	0.9999
	1/1600	-1.1612	1.12104E-04		-1.16128	3.58460E-05	_	-1.16129	1.82967E-05	_
$\frac{\partial\phi}{\partial Y}(0.25,0)$	1/100	-1.2706	3.89979E-03	1.0780	-1.2734	1.03682E-03	1.0183	-1.27393	5.43035E-04	1.1505
	1/200	-1.2726	1.84729E-03	1.0742	-1.2740	5.11870E-04	1.1284	-1.27423	2.44618E-04	1.3586
	1/400	-1.2736	8.77329E-04	1.1087	-1.2742	2.34148E-04	1.3566	-1.27438	9.53903E-05	2.1989
	1/800	-1.2741	4.06842E-04	1.2149	-1.2744	9.14318E-05	2.2574	-1.27445	2.07759E-05	0.3298
	1/1600	-1.2743	1.75269E-04	_	-1.2745	1.91234E-05	_	-1.27449	1.65299E-05	_
$\phi$ (1, 0)	1/100	0.5431	1.57930E-03	0.9957	0.54199	5.10919E-04	1.0000	0.54174	2.60089E-04	1.0000
	1/200	0.5423	7.91982E-04	0.9979	0.54173	2.55457E-04	1.0000	0.54161	1.30044E-04	1.0000
	1/400	0.5419	3.96571E-04	0.9989	0.54160	1.27728E-04	1.0000	0.54154	6.50218E-05	1.0000
	1/800	0.5417	1.98430E-04	0.9995	0.54154	6.38633E-05	0.9999	0.54151	3.25110E-05	1.0000
	1/1600	0.5416	9.92512E-05	—	0.54151	3.19331E-05	—	0.54149	1.62561E-05	—
Average current density at Y = 0 $\frac{1}{0.5} \int_{X=0}^{X=0.5} \frac{\partial \phi}{\partial Y} dX$	1/100	-1.532	1.24497E-01	0.4095	-1.589	6.77950E-02	0.3515	-1.605	5.19807E-02	0.3115
$0.5 J X=0  \partial Y$	1/200	-1.563	9.37319E-02	0.3878	-1.603	5.31338E-02	0.3156	-1.615	4.18864E-02	0.2713
	1/400	-1.585	7.16365E-02	0.3591	-1.614	4.26951E-02	0.2754	-1.622	3.47060E-02	0.2293
	1/800	-1.601	5.58507E-02	0.3242	-1.621	3.52752E-02	0.2333	-1.627	2.96067E-02	0.1880
	1/1600	-1.612	4.46105E-02	_	-1.626	3.00082E-02	_	-1.631	2.59898E-02	_

Table I. Error and convergence analysis using different shape functions in FEM for the PCD (Model 1).

a) Analytical solution:  $\frac{\partial \phi}{\partial Y}(0, 0) = -1.16131153023325, \frac{\partial \phi}{\partial Y}(0.25, 0) = -1.27447197226800, \phi(1, 0) = 0.54147517960447, \frac{1}{0.5} \int_{X=0}^{X=0.3} \frac{\partial \phi}{\partial Y} \Big|_{Y=0} dX = -1.65650764877779.$ 

Variable of Interest	Element Size $h_x = h_y$ = h	Bilinear			Biquadratic			Bicubic		
		Numerical Solution	$\begin{array}{l} & \text{Error} \\ & E_r = \\  \text{Numerical} \\ & \text{solution (h/2)} \\ & - & \text{Numerical} \\ & \text{solution (h)}   \end{array}$	Order of Convergence $\log_2\left(\frac{E_r(h)}{E_r(h/2)}\right)$	Numerical Solution	Error $E_r =$  Numerical so- lution (h/2)— Numerical solution (h)	Order of Convergence $\log_2\left(\frac{E_r(h)}{E_r(h/2)}\right)$	Numerical Solution	$\begin{array}{l} & \text{Error} \\ & E_r = \\  \text{Numerical} \\ & \text{solution (h/2)} \\ & - & \text{Numerical} \\ & \text{solution (h)}   \end{array}$	Order of Convergence $\log_2\left(\frac{E_r(h)}{E_r(h/2)}\right)$
$\phi$ (0, 0)	1/100	0.4137893	4.39099E-06	1.8792	0.41378348	1.34207E-07	1.9981	0.4137833463	3.19863E-08	2.0033
	1/200	0.4137849	1.19365E-06	1.8883	0.41378335	3.35960E-08	1.9920	0.4137833143	7.97813E-09	2.0656
	1/400	0.4137837	3.22431E-07	1.8962	0.41378331	8.44555E-09	2.0690	0.4137833063	1.90590E-09	3.0835
	1/800	0.4137834	8.66232E-08	_	0.41378331	2.01280E-09	_	0.4137833044	2.24835E-10	
	1/1600	0.4137833	_	_	0.41378330		_	0.4137833042	_	_
$\phi$ (0.25, 0)	1/100	0.3973398	5.22660E-06	1.8732	0.397332849	1.67992E-07	1.9964	0.3973326779	4.01044E-08	2.0026
	1/200	0.3973346	1.42667E-06	1.8831	0.397332681	4.21036E-08	1.9918	0.3973326377	1.00080E-08	2.0514
	1/400	0.3973332	3.86767E-07	1.8917	0.397332638	1.05856E-08	2.0538	0.3973326277	2.41450E-09	2.7983
	1/800	0.3973328	1.04231E-07	_	0.397332628	2.54962E-09	_	0.3973326253	3.47092E-10	
	1/1600	0.3973327	_	_	0.397332625		_	0.3973326250	_	_
$\phi$ (0.5, 0)	1/100	0.3098369	9.79922E-06	1.7146	0.3098239	7.47130E-07	1.8649	0.309823112	2.00799E-07	1.8804
	1/200	0.3098271	2.98578E-06	1.7403	0.3098231	2.05119E-07	1.8745	0.309822912	5.45398E-08	1.8982
	1/400	0.3098241	8.93639E-07	1.7618	0.3098229	5.59391E-08	1.9068	0.309822857	1.46323E-08	2.0020
	1/800	0.3098232	2.63507E-07	_	0.3098229	1.49183E-08	_	0.309822842	3.65311E-09	_
	1/1600	0.3098229	_	_	0.3098228	_	_	0.309822839	_	_
φ (1, <b>0</b> )	1/100	0.1938271	4.14280E-06	1.8211	0.19382163	1.91348E-07	1.9992	0.193821434	4.55464E-08	2.0024
	1/200	0.1938230	1.17242E-06	1.8407	0.19382144	4.78630E-08	1.9884	0.193821389	1.13676E-08	2.0519
	1/400	0.1938218	3.27314E-07	1.8564	0.19382139	1.20623E-08	2.3526	0.193821377	2.74145E-09	2.8430
	1/800	0.1938215	9.03931E-08	_	0.19382138	2.36166E-09	_	0.193821375	3.82071E-10	_
	1/1600	0.1938214	_	_	0.19382137	_	_	0.193821374	_	_
Average current	1/100	-0.600	5.39258E-03	0.8100	-0.6106	8.71790E-04	0.9952	-0.61162	3.59484E-04	0.9990
density at Y = 0 $\frac{1}{0.5} \int_{X=0}^{X=0.5} \frac{\partial \phi}{\partial Y} dX$										
	1/200	-0.605	3.07586E-03	0.8319	-0.6115	4.37341E-04	0.9972	-0.61198	1.79862E-04	0.9995
	1/400	-0.609	1.72796E-03	0.8494	-0.6119	2.19091E-04	0.9984	-0.61216	8.99612E-05	0.9998
	1/800	-0.610	9.59063E-04	_	-0.6121	1.09665E-04	_	-0.61225	4.49880E-05	_
	1/1600	-0.611	_	_	-0.6122	_	_	-0.61230	_	_

Table II. Error and convergence analysis using different shape functions in FEM for the SCD (Model 2).

Typically, dynamics are important for the electrolyte distribution. There are mainly two different ways to model electrolyte transport dynamics, namely dilute and concentrated solution theories.<sup>4</sup> With the electroneutrality and equal species diffusivity assumptions for a binary electrolyte, using dilute solution theory, the governing equations and boundary conditions are given by *Model 4*.

Model 4

$$\begin{aligned} \frac{\partial c}{\partial \tau} &= \left(\frac{L_Y^2}{L_x^2}\right) \frac{\partial^2 c}{\partial X^2} + \frac{\partial^2 c}{\partial Y^2} \\ \left(\frac{L_Y^2}{L_x^2}\right) \left(c\frac{\partial^2 \phi}{\partial X^2}\right) + c\frac{\partial^2 \phi}{\partial Y^2} + \left(\frac{L_Y^2}{L_x^2}\right) \left(\frac{\partial \phi}{\partial X \partial X}\frac{\partial c}{\partial Y}\right) + \frac{\partial c}{\partial Y}\frac{\partial \phi}{\partial Y} = 0 \\ \frac{\partial c}{\partial X} &= 0 \\ \frac{\partial \phi}{\partial X} &= 0 \\ \end{bmatrix} \text{at } X = 0, \ 1; \ \frac{\phi = 0}{-\frac{\partial c}{\partial Y}} + c\frac{\partial \phi}{\partial Y} = 0 \\ \end{bmatrix} \text{at } Y = 1 \\ \begin{pmatrix} \frac{\phi = 1}{(\frac{\partial c}{\partial Y} + c\frac{\partial \phi}{\partial Y})} = 2\int_{Y=1,X=0}^{Y=1,X=1} \left(\frac{\partial c}{\partial Y} + c\frac{\partial \phi}{\partial Y}\right) \text{d} X \\ \frac{\partial \phi}{\partial Y} &= 0 \\ \frac{\partial \phi}{\partial Y} &= 0 \\ \end{bmatrix} \text{at } Y = 0, \ 0.5 < X \leqslant 1 \\ c = 1 \\ \phi &= 0 \\ \end{bmatrix} \text{for } X, \ Y \text{ at } \tau = 0 \end{aligned}$$
[10]

At the electrode at Y = 0, the cation flux is set to the average value at the top of the domain. An additional error arises from the use of time integrator in simulating this model.

**Poisson Nernst Planck (PNP) model**—The electroneutrality assumption is not applicable for interfaces close to the electrodes.<sup>12</sup> Even for a 1D problem, the PNP model is difficult to solve to high precision near the electrodes.<sup>13</sup> This suggests that incorporating the PNP into 2D models with singularity in the domains of interest cannot be currently resolved to machine precision easily. A well-defined model with time dynamics and boundary conditions for the domain studied can be written in the scaled form as:

## Model 5

$$\begin{split} & \frac{\partial \mathbf{C}}{\partial \tau} = \left(\frac{\mathbf{L}_{\mathbf{Y}}^2}{\mathbf{L}_{\mathbf{X}}^2}\right) \frac{\partial \left(\frac{\partial \mathbf{C}}{\partial \mathbf{X}} + \rho \frac{\partial \phi}{\partial \mathbf{X}}\right)}{\partial \mathbf{X}} + \frac{\partial \left(\frac{\partial \mathbf{C}}{\partial \mathbf{Y}} + \rho \frac{\partial \phi}{\partial \mathbf{Y}}\right)}{\partial \mathbf{Y}} \\ & \frac{\partial \rho}{\partial \tau} = \left(\frac{\mathbf{L}_{\mathbf{Y}}^2}{\mathbf{L}_{\mathbf{X}}^2}\right) \frac{\partial \left(\frac{\partial \rho}{\partial \mathbf{X}} + \mathbf{C} \frac{\partial \phi}{\partial \mathbf{X}}\right)}{\partial \mathbf{X}} + \frac{\partial \left(\frac{\partial \rho}{\partial \mathbf{Y}} + \mathbf{C} \frac{\partial \phi}{\partial \mathbf{Y}}\right)}{\partial \mathbf{Y}} \\ & \left(\frac{\mathbf{L}_{\mathbf{Y}}^2}{\mathbf{L}_{\mathbf{X}}^2}\right) \frac{\partial^2 \phi}{\partial \mathbf{Y}^2} + \frac{\partial^2 \phi}{\partial \mathbf{Y}^2} = -\frac{\rho}{\varepsilon^2} \\ & \frac{\partial c}{\partial \mathbf{X}} + \rho \frac{\partial \phi}{\partial \mathbf{X}} = 0 \\ & \frac{\partial \rho}{\partial \mathbf{X}} + \mathbf{C} \frac{\partial \phi}{\partial \mathbf{X}} = 0 \\ & \frac{\partial \phi}{\partial \mathbf{X}} = 0 \\ & -\left(\frac{\partial \mathbf{C}}{\partial \mathbf{Y}} + \rho \frac{\partial \phi}{\partial \mathbf{Y}}\right) = \mathbf{i}_{0,\text{scaled}} \sinh\left(\frac{\eta}{2}\right) \\ & -\left(\frac{\partial \rho}{\partial \mathbf{Y}} + \mathbf{C} \frac{\partial \phi}{\partial \mathbf{Y}}\right) = \mathbf{i}_{0,\text{scaled}} \sinh\left(\frac{\eta}{2}\right) \\ & \eta = \mathbf{V}_{\text{anode}} - \phi = 1 - \phi \\ & 1 - \phi = -\delta \varepsilon \frac{\partial \phi}{\partial \mathbf{Y}} \end{split} \right\}$$
 at  $\mathbf{Y} = 0, \ 0 \leqslant \mathbf{X} \leqslant 0.5$ 

$$\begin{aligned} \frac{\partial C}{\partial Y} &+ \rho \frac{\partial \phi}{\partial Y} = 0\\ \frac{\partial \rho}{\partial Y} &+ C \frac{\partial \phi}{\partial Y} = 0\\ \frac{\partial \phi}{\partial Y} &= 0 \end{aligned} \right\} \text{ at } Y = 0, \ 0.5 < X \leqslant 1\\ \left(\frac{\partial C}{\partial Y} &+ \rho \frac{\partial \phi}{\partial Y}\right) &= \left(\frac{1}{2}\right) \int_{Y=0,X=0}^{Y=0,X=0.5} \left(\frac{\partial C}{\partial Y} &+ \rho \frac{\partial \phi}{\partial Y}\right) dX\\ \left(\frac{\partial \rho}{\partial Y} &+ C \frac{\partial \phi}{\partial Y}\right) &= \left(\frac{1}{2}\right) \int_{Y=0,X=0}^{Y=0,X=0.5} \left(\frac{\partial \rho}{\partial Y} &+ C \frac{\partial \phi}{\partial Y}\right) dX\\ \phi &= 0 \end{aligned} \right\} \text{ at } Y = 1\\ \phi &= 0\\ C = 1\\ \rho &= 0\\ \phi &= 0 \end{aligned}$$
 for X, Y at  $\tau = 0$ 

$$\end{aligned}$$

where the dimensionless species concentrations, expressed in terms of "average concentration" and "net charge density", are given by

$$C = \frac{c_1 + c_2}{2}; \ \rho = \frac{c_1 - c_2}{2}$$
[12]

The Poisson's equation introduces a parameter  $\varepsilon = \lambda_D/L_y$ , which is the ratio of the thickness of the electrical double layer to the characteristic length scale of the system. Net electroneutrality is assumed, which is reasonable for most practical cases with  $\varepsilon \ll 1$ .<sup>14</sup>

*Moving boundary*—The simple model for the potential in *Model* 3 can be modified to a moving boundary (MB) problem as solved earlier for the electrodeposition problem by Alkire et al.<sup>15</sup> The problem statement is described as:

$$\begin{cases} \left(\frac{L_{y}^{2}}{L_{x}^{2}}\right)\frac{\partial^{2}\phi}{\partial X^{2}} + \frac{\partial^{2}\phi}{\partial Y^{2}} = 0 \\ \frac{\partial\phi}{\partial X} = 0 \text{ at } X = 0, 1 \\ \phi = 0 \text{ at } Y = 1 \\ -\nabla\phi \cdot n = 2i_{0,\text{scaled}} \sinh\left(\frac{\eta}{2}\right) \\ -\frac{\partial s}{\partial \tau} = 2i_{0,\text{scaled}} \sinh\left(\frac{\eta}{2}\right) \\ \eta = \text{V}_{\text{anode}} - \phi = 1 - \phi \\ n = n_{x}\hat{i} + n_{y}\hat{j} \\ n_{x} = -\frac{\left(\frac{L_{y}}{L_{x}}\right)\frac{\partial s}{\partial X}}{\sqrt{1 + \left(\frac{L_{y}}{L_{x}}\right)^{2}\left(\frac{\partial s}{\partial X}\right)^{2}}} \\ n_{Y} = \frac{1}{\sqrt{1 + \left(\frac{L_{y}}{L_{x}}\right)^{2}\left(\frac{\partial s}{\partial X}\right)^{2}}} \\ -\frac{\partial s}{\partial \tau} = -\nabla\phi \cdot n = 0 \\ n = n_{x}\hat{i} + n_{y}\hat{j} \\ n_{x} = 0 \\ n_{Y} = 1 \end{cases} \right\} \text{ at } Y = 0, \ 0.5 < X \leqslant 1 \\ n_{x} = 0 \\ n_{Y} = 1 \end{cases}$$
 at  $Y = 0, \ 0.5 < X \leqslant 1 \\ 13 \end{cases}$ 

where electrochemical reaction occurs at Y = 0 at  $\tau = 0$ . The velocity of the MB is related to the normal component of the local electrostatic potential gradient.

This well-defined problem can be used to march forward in time to see how the morphology changes with time. This front-capturing method involves re-meshing the domain of interest. Phase-field and level-set methods are alternatives that avoid remeshing when the boundary has moved.<sup>16–18</sup> These methods retain the original domain of interest and modify the models to include a source term in the equation, which handles the transition from one phase to another. In addition, different transport properties (D) are used in different phases. A very simple way to demonstrate this approach is the 1D model.

Model 7a

$$\begin{aligned} \frac{\partial \mathbf{c}}{\partial \tau} &= \frac{\partial^2 \mathbf{c}}{\partial X^2} \\ \frac{\partial \mathbf{c}}{\partial \mathbf{X}} &= \delta \text{ at } \mathbf{X} = \mathbf{0} \\ \mathbf{c} &= 1 \text{ at } \mathbf{X} = \mathbf{1} \\ \mathbf{c} &= 1 \text{ at } \tau = \mathbf{0} \text{ for all } \mathbf{X} \end{aligned}$$
 [14]

Applying a cell-centered finite difference scheme, *Model 7a* can be discretized as

$$\frac{dc_{i}(\tau)}{d\tau} = \frac{c_{i+1}(\tau) - 2c_{i}(\tau) + c_{i-1}(\tau)}{h^{2}} \ 1 \leqslant i \leqslant N$$

$$c_{i}(0) = 1$$

$$c_{1}(\tau) - c_{0}(\tau) = \delta h$$

$$c_{N}(\tau) + c_{N+1}(\tau) = 2$$
[15]

This model can be modified by moving the inhomogeneous boundary condition to the bulk of governing equation as: *Model 7b* 

$$\begin{aligned} \frac{\partial \mathbf{c}}{\partial \tau} &= \mathbf{D} \frac{\partial^2 \mathbf{c}}{\partial X^2} + \mathbf{R} \\ \mathbf{D} &= \begin{cases} 0 & \mathbf{X} = 0 \\ 1 & 0 < \mathbf{X} \leqslant 1 \end{cases} \\ \mathbf{R} &= \begin{cases} -\frac{\delta}{\mathbf{h}} & 0 \leqslant \mathbf{X} < \mathbf{h} \\ 0 & \mathbf{h} \leqslant \mathbf{X} \leqslant 1 \end{cases} \end{aligned}$$
[16]

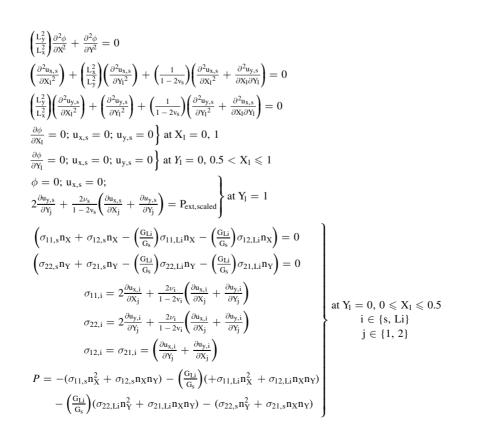
Both models result in the same equations to be solved for time integration. High values of  $\delta$  typically require a small mesh size (h). If h is small, the reaction term R becomes very high. When the boundary moves with time, the parameters (D, R) and time stepping must be carefully handled.

All the methods are approximate at the moving interface, and more accurate away from the moving interface.<sup>18</sup> For analytically defined moving boundaries, front-capturing methods are more accurate than front-tracking methods. If the moving boundaries are complicated and the numerical resolution is poor, front-tracking methods may be more convenient, but the potential efficiency gained from front-capturing methods can be significant. All the methods are likely to require very fine meshes close to the electrodes.<sup>18</sup>

*Microscale effects*—Newman's porous electrode theory models a porous electrode consisting of solid and liquid phase in an average sense. As a result, when detailed models are developed for both solid and liquid phases, with no source terms and averaged along the y-direction, the reaction at the solid-liquid interface becomes a source term. Detailed micro-scale electrode models can be more accurate, specifically due to their ability to correlate effective transport properties in p2D type models with electrode morphology.<sup>19</sup> A recent article suggests that FEM and FVM arrive at different values for effective property calculations from micro-scale models, suggesting that grid convergence (in particular to machine precision) is perhaps not possible.<sup>20</sup> Phase-separation dynamics in electrode particles are yet another class of physics that result in numerical challenges.<sup>21,22</sup>

We now present some examples.

*Pressure models—kinetics*—The simple 2D model for  $\phi$  with kinetics can be coupled with detailed pressure models, typically for the purpose of modifying the kinetics at the surface of the electrode.<sup>23,24</sup> The problem formulation is given as: *Model 8a* 



[17]

where the externally applied pressure is scaled with  $G_s$  as  $P_{ext,scaled} = \frac{P_{ext}}{G_s}$ . The MB equations are specified as a separate sub-model:

M. J.1 01

$$\begin{split} \frac{\partial s_x}{\partial \tau} &= -2 \left( \frac{L_y}{L_x} \right) i_{0,\text{def}} \sinh\left(\frac{\eta}{2}\right) n_X; \ \frac{\partial s_y}{\partial \tau} &= -2i_{0,\text{def}} \sinh\left(\frac{\eta}{2}\right) n_Y \\ n_X &= -\frac{\left(\frac{L_y}{L_x}\right) \frac{\partial s_y}{\partial \chi_l} + \left(\frac{L_y}{L_x}\right) \frac{\partial u_{y,s}}{\partial \chi_l}}{\sqrt{\left(1 + \frac{\partial s_x}{\partial \chi_l} + \frac{\partial u_{x,s}}{\partial \chi_l}\right)^2 + \left(\left(\frac{L_y}{L_x}\right) \frac{\partial s_y}{\partial \chi_l} + \left(\frac{L_y}{L_x}\right) \frac{\partial u_{y,s}}{\partial \chi_l}}\right)^2}; \\ n_Y &= \frac{1 + \frac{\partial s_x}{\partial \chi_l} + \frac{\partial u_{x,s}}{\partial \chi_l}}{\sqrt{\left(1 + \frac{\partial s_x}{\partial \chi_l} + \frac{\partial u_{x,s}}{\partial \chi_l}\right)^2 + \left(\left(\frac{L_y}{L_x}\right) \frac{\partial s_y}{\partial \chi_l} + \left(\frac{L_y}{L_x}\right) \frac{\partial u_{y,s}}{\partial \chi_l}}\right)^2}}{\sqrt{\left(1 + \frac{\partial s_x}{\partial \chi_l} + \frac{\partial u_{x,s}}{\partial \chi_l}\right)^2 + \left(\left(\frac{L_y}{L_x}\right) \frac{\partial s_y}{\partial \chi_l} + \left(\frac{L_y}{L_x}\right) \frac{\partial u_{y,s}}{\partial \chi_l}}\right)^2}} \\ \eta &= V_{\text{anode}} - \phi = 1 - \phi \end{split}$$

where  $u_{x,s}$  and  $u_{y,s}$  are the scaled x and y-components of the displacement, respectively.

The scaled exchange current density i<sub>0,scaled</sub> is modified as

$$i_{0,def} = i_{0,scaled} e^{-\beta P}$$
  

$$\beta = -G_s \varsigma$$
  

$$\varsigma = \frac{\overline{V_{Li} - (1 - t_0^+) \overline{V_{LiX}}}}{4RT}$$
[19]

where P denotes scaled value of the hydrostatic pressure at the electrodeelectrolyte interface and  $\beta$  is a dimensionless enhancement factor.

The deformation of the Li metal is given by *Model 8c*, expressed in a separate coordinate system  $(X_2, Y_2)$ .

### Model 8c

$$\begin{pmatrix} \frac{\partial^2 u_{x,Li}}{\partial X_2^2} \end{pmatrix} + \begin{pmatrix} \frac{L_x^2}{L_y^2} \end{pmatrix} \begin{pmatrix} \frac{\partial^2 u_{x,Li}}{\partial Y_2^2} \end{pmatrix} + \begin{pmatrix} \frac{1}{1-2v_{Li}} \end{pmatrix} \begin{pmatrix} \frac{\partial^2 u_{x,Li}}{\partial X_2^2} + \frac{\partial^2 u_{y,Li}}{\partial X_2 \partial Y_2} \end{pmatrix} = 0$$

$$\begin{pmatrix} \frac{L_y^2}{L_x^2} \end{pmatrix} \begin{pmatrix} \frac{\partial^2 u_{y,Li}}{\partial X_2^2} \end{pmatrix} + \begin{pmatrix} \frac{\partial^2 u_{y,Li}}{\partial Y_2^2} \end{pmatrix} + \begin{pmatrix} \frac{1}{1-2v_{Li}} \end{pmatrix} \begin{pmatrix} \frac{\partial^2 u_{y,Li}}{\partial Y_2^2} + \frac{\partial^2 u_{x,Li}}{\partial X_2 \partial Y_2} \end{pmatrix} = 0$$

$$u_{x,Li} = 0; \ u_{y,s} = 0 \ \text{at} \ X_2 = 1$$

$$u_{x,Li} = u_{x,s}; \ u_{y,Li} = u_{y,s} \ \text{at} \ Y_2 = 0, \ 0 \leqslant X_2 \leqslant 0.5$$

$$u_{x,Li} = 0; \ u_{y,Li} = 0 \ \text{at} \ Y_2 = -s_y, \ 0 \leqslant X_2 \leqslant 0.5$$

$$[20]$$

Porous electrodes—Tortuosity—Assuming that the solid particles are perfect spheres, simplified spatially resolved micro-scale model equations for the electrolyte and particle phases are given by Models 9a and 9b, respectively:

Model 9a—Electrolyte phase

$$\begin{split} \frac{\partial c}{\partial \tau} &= \left(\frac{L_{Y}^{2}}{L_{x}^{2}}\right) \frac{\partial^{2} c}{\partial X^{2}} + \frac{\partial^{2} c}{\partial Y^{2}} \\ \left(\frac{L_{Y}^{2}}{L_{x}^{2}}\right) \left(c\frac{\partial^{2} \phi}{\partial X^{2}}\right) + c\frac{\partial^{2} \phi}{\partial Y^{2}} + \left(\frac{L_{Y}^{2}}{L_{x}^{2}}\right) \left(\frac{\partial \phi}{\partial X} \frac{\partial c}{\partial X}\right) + \frac{\partial c}{\partial Y} \frac{\partial \phi}{\partial Y} = 0 \\ \frac{\partial c}{\partial X} &= 0 \\ \frac{\partial \phi}{\partial X} &= 0 \\ \frac{\partial c}{\partial Y} &= 0 \\ \frac{\partial c}{\partial Y} &= 0 \\ \frac{\partial \phi}{\partial Y} &= 0 \\ \frac{\partial \phi}{\partial Y} &= 0 \\ \frac{\partial c}{\partial Y} &= 0 \\ \frac{\partial$$

$$\left. \begin{array}{l} \text{at } Y_1 \,=\, 0, \quad 0 \,\leqslant\, X_1 \,\leqslant\, 0.5 \end{array} \right. \end{tabular} \tag{18}$$

### Model 9b—Particle phase

$$\begin{split} & \frac{\partial c_{x,i}}{\partial r} = \left(\frac{D_{x}L_{y}^{2}}{D_{x}^{2}}\right) \frac{1}{R^{2}} \frac{\partial}{\partial R} \left(R^{2} \frac{\partial c_{x,i}}{\partial R}\right) \\ & -\frac{D_{x}}{R_{p}} \frac{\partial c_{x,i}}{\partial R} = \frac{i_{B} v_{,surf,avg}}{F} \\ & i_{B} v_{,surf} = 2i_{0,ert} c^{0.5} (c_{s,i})^{0.5} (c_{s,max} - c_{s,i})^{0.5} \sinh\left(\frac{\eta_{i}}{2}\right) \\ & at R = 1 \text{ and } 1 \leqslant i \leqslant N_{P} \\ & \eta_{i} = \phi_{s}(\tau) - \phi - U(c_{s,i}) \\ & i_{B} v_{,surf,avg,i} = \frac{1}{2\pi} \int_{\theta=0}^{\theta=2\pi} i_{B} v_{,surf}(\theta) d\theta \\ & \frac{\partial c_{x,i}}{\partial R} = 0 \text{ at } R = 0 \text{ and } 1 \leqslant i \leqslant N_{P} \\ & -\frac{D_{x}}{R_{p}} \frac{\partial c_{x,i}}{\partial R} = N_{+,surf,avg,i}; N_{+,surf,avg,i} \\ & = \frac{1}{2\pi} \int_{\theta=0}^{\theta=2\pi} N_{+,surf,avg,i}; d\theta = -\frac{D_{x}}{R_{p}} \frac{\partial c_{x,i}}{\partial R} \\ & N_{+,surf} = \left(-\frac{Dc_{0}}{L_{x}}\right) \frac{\partial c}{\partial x} n_{X,i} - \left(\frac{Dcc_{0}}{L_{y}}\right) \frac{\partial \phi}{\partial x} n_{X,i} \\ & - \left(\frac{Dc_{0}}{L_{y}}\right) \frac{\partial c}{\partial x} n_{X,i} - \left(\frac{Dcc_{0}}{L_{y}}\right) \frac{\partial \phi}{\partial y} n_{Y,i} \\ & i_{2,surf,i} = -\left(\frac{2EDcc_{0}}{L_{x}}\right) \frac{\partial \phi}{\partial x} n_{X,i} - \left(\frac{2EDcc_{0}}{L_{y}}\right) \frac{\partial \phi}{\partial y} n_{Y,i} \\ & i_{2,surf,i} = i_{B} v_{,surf,avg,i} = \frac{1}{2\pi} \int_{\theta=0}^{\theta=2\pi} i_{2,surf,i} d\theta \\ & X = X_{c,i} + \left(\frac{R_{p}}{L_{x}}\right) \cos(\theta); Y = Y_{c,i} + \left(\frac{R_{p}}{L_{y}}\right) \sin(\theta) \\ & n_{X,i} = \frac{X_{c,i} + \left(\frac{R_{p}}{L_{x}}\right) \cos(\theta)}{\sqrt{\left(X_{c,i} + \left(\frac{R_{p}}{L_{x}}\right) \cos(\theta)\right)^{2} + \left(Y_{c,i} + \left(\frac{R_{p}}{L_{y}}\right) \sin(\theta)}\right)^{2}} \\ & i_{tot} = 2\pi R_{p} \sum_{i=1}^{N_{p}} i_{B} v_{,surf,avg,i}; - \left(\frac{L_{x} PDcc_{0}}{L_{y}}\right) \frac{\partial \phi}{\partial Y} \Big|_{Y=0} = i_{tot} \end{aligned}$$

where the subscript i is used to denote the ith solid particle, and Np denotes the total number of solid particles in the domain.

The two sub-models are coupled through the boundary conditions at the particle surfaces with all of the electrolyte phase variables applied in an average sense along the particle circumference. A uniform solid-phase potential  $\phi_s(\tau)$  is also assumed.

Simulation and numerical aspects-This section briefly states the important numerical and simulation aspects relevant for solving the models described, and in general for battery models. Each of the topics can be a separate critical review by itself, and only few personal perspectives are mentioned here.

*Spatial discretization*—Only FEM is discussed in depth for *Models 1* and 2. Many spatial discretization methods exist, including finite difference methods (constant grid, variable grid, higher order), finite volume methods, spectral methods, and global and local FEM (strong form, weak form, orthogonal collocation). All these methods result in a system of algebraic equations for steady-state models, and a system of differential-algebraic equations (DAEs) for models with time dynamics. Adaptive meshing can be used for the spatial discretization of the domain.

*Linear solver*—A linear solver plays a critical role in the simulation of battery models. Even for the simple linear problems (*Models 1* and 2), direct sparse solvers can be used only up to 1000  $\times$  1000 elements, after which multigrid iterative methods are more efficient, which require solving the model repeatedly with different element sizes.<sup>25</sup> Gaussian elimination<sup>26</sup> used in the early days is replaced by banded solvers,<sup>27</sup> particularly for one-dimensional PDEs. For 2D problems, banded solvers are not optimal, and sparse iterative and direct solvers are used.<sup>28</sup> COMSOL Multiphysics recommends the use of sparse direct solvers up to 500,000 degrees of freedom (DOFs).<sup>25</sup> GMRES and iterative solvers are preferred for larger number of DOFs. For Krylov-type efficient iterative solvers, good preconditioners are needed.<sup>28</sup> Often, knowing the physics of the problem and solving a simpler problem helps in identifying a good preconditioner.

*Time-integrators*—Discretization of battery models results in stiff partial differential algebraic equations (PDAEs). Once the spatial discretization is chosen, the resulting set of DAEs can be integrated in time with adaptive solvers using Method of Lines (MOL).<sup>29</sup> There are multiple variations, possibilities, and demands for these solvers. For example, Backward difference methods (BDF),<sup>30–32</sup> as implemented in DASPK and IDA, offer efficient simulation of index-1 DAE arising from PNP equations (*Model 4*). *Model 3* is strictly an index-2 DAE (if electroneutrality is not used to eliminate one of the concentration variables), which is best solved using RADAU5, an implicit Runge–Kutta method.<sup>33</sup>

It should be noted that a particular spatial discretization approach providing a particular order of accuracy for steady-state models may not provide the same order of accuracy in a MOL framework. In addition, all the time-integrators will not provide the expected order of accuracy in temporal discretization for the numerical simulation of PDAEs, in particular close to the boundaries, which are of interest for battery models. For example, while BDF methods can integrate stiff DAEs, the same approach, when used for temporal discretization in a simultaneous approach framework, loses order of accuracy (and yields unstable results) even for simple ODEs.<sup>34</sup>

*Programming environment*—Implementation of a particular algorithm in C++, C or FORTRAN is likely to be more efficient compared to implementation in user-friendly platforms such as Maple or MATLAB. However, the learning curve for beginners is steeper. The platform and software used have effects on computational efficiency of a particular algorithm. While C can be faster than MATLAB, the A\b command in MATLAB seems to be well optimized for large-scale systems compared to open-source linear solvers. Some of the robust linear solvers/DAE solvers have restrictive licenses.

*Boundary conditions*—When micro-scale models are used in the literature, it is a common practice to use a bulk condition for the electrolyte away from the domain of interest. A bulk flux condition is more appropriate as that will conserve mass. Some of the past work involves resolving the boundary layers by developing approximate boundary conditions.<sup>4,35</sup> High rates typically mean non-uniform current distributions, and both macro- and micro-scale models should be ideally solved without approximations. Even for the standard p2D models, for galvanostatic conditions, specifying

solid- or liquid-phase potential to a particular value is required for the model to be well-posed for simulation. While the location for specifying the potential value is arbitrary, this has a subtle but important effect in optimizing simulation algorithms for robustness and efficiency depending on the discretization scheme used.

Battery management system (BMS) and real-time control-Recently, detailed models have been solved in real-time for control and design purposes.<sup>36–43</sup> This was built on decades of research from multiple teams applying best possible algorithms for discretization in x, t and careful mathematical analysis to reduce the number of states. This progress was facilitated by (1) a detailed model and open-source code published in 1993 by Newman's group,<sup>44</sup> (2) multiple groups attempted to simulate the same model more efficiently by introducing different reformulation and model reduction approaches,<sup>45–52</sup> and (3) the battery community applied (1) and (2) for validating model predictions with experimental data for a wide range of applications, chemistries, and form-factors.<sup>53,54</sup> A similar approach is possible for detailed 2D and micro-scale models but will probably require many additional mathematical techniques and validation. For example, moving to the conformed coordinate enables higher order of accuracy for Model 2 using FEM or any spatial discretization approach. Similarly, Richardson extrapolation can provide 6 digits of accuracy for *Model 1* even with less than  $300 \times 300$  elements.

Parameter estimation and system engineering approaches require fast, efficient, and robust simulation of models. Many of the transport and kinetic parameters in the battery models are nonlinear and strongly affect the performance of batteries. The two main optimization-based methods for estimation and control are simultaneous and sequential approaches. If the underlying numerical scheme is not accurate enough, any method used to estimate parameters or perform optimal control (Bayesian estimation, MCMC, offline and online optimal control, surrogate model development) will likely fail or provide sub-optimal results. Even a gain of 0.01% per cycle will have a significant impact on battery performance. Machine precision is not needed as instruments have error in measurement; however, efficient and robust simulation to arrive at a relative tolerance of 1E-6 for the variables (and sensitivities with respect to parameters) requires careful analysis of different algorithms. Speed is essential in optimization- and modelbased BMS frameworks for batteries that require real-time simulations for more than 1000s of cycles with different possible operating protocols.

## **Conclusions and Future Needs**

At first, two simple 2D models, for primary and secondary current distributions, are presented and solved using FEM. These simple models suggest the critical need for grid convergence analysis. These models were modified to incorporate additional mechanisms and physics. Detailed, stand-alone, and well-defined models are provided as examples for numerical analysts to benchmark accuracy, and computational efficiency. Our recommendations are

- Perform and provide rigorous grid convergence results and mention the precision obtained. This grid convergence exercise should be performed at multiple locations in the domain.
- (2) Use finer mesh near the singular points and coarser mesh away from the singular points. In addition, use lower order methods near the singular points and higher order methods elsewhere.
- (3) Ideally, solve any multiscale model at least with two different methods to make sure the results have converged at least qualitatively.
- (4) Pay attention to every numerical detail for best possible efficiency and robustness—method for spatial discretization, method for time-integration, linear solver, method for Jacobian calculation, software and hardware environment, etc. The list of considerations is long, and answered best using the global

objective in hand, e.g., does the potential (or fade, power etc.) predicted by the model match the experimental data?

We strongly encourage careful calculation and analysis of the (5)numerical error considering all different sources of error, explicitly providing these values, precisely defining the error calculated, and possibly providing details in a separate section. The error should be calculated with respect to an analytical solution wherever possible.

A webpage with numerical methods and results will be maintained by VS. Link to the extended arXiv version of this article can be found on the same webpage. URL: http://sites.utexas.edu/maple/ challenges-in-moving-to-multiscale-battery-models-where-electrochemistry-meets-and-demands-more-from-math/.

#### Acknowledgments

The authors would like to thank the U.S. Department of Energy (DOE) for providing financial support for this work through Advanced Battery Material Research (BMR) Program (Battery 500 Consortium). The authors would also like to acknowledge support from Accelerated Materials Discovery and Design Program of the Toyota Research Institute through the D3BATT center on Data-Driven Design of Rechargeable Batteries.

#### ORCID

Krishna Shah () https://orcid.org/0000-0002-7802-6361 Akshay Subramaniam (D https://orcid.org/0000-0002-9306-7436 Lubhani Mishra Dhttps://orcid.org/0000-0003-2135-9381 Taejin Jang (1) https://orcid.org/0000-0003-4279-8455 Venkat R. Subramanian in https://orcid.org/0000-0002-2092-9744

#### References

- 1. M. Tang, P. Albertus, and J. Newman, J. Electrochem. Soc., 156, A390 (2009).
- 2. K. N. Wood, E. Kazyak, A. F. Chadwick, K. H. Chen, J. G. Zhang, K. Thornton, and N. P. Dasgupta, ACS Cent. Sci., 2, 790 (2016).
- 3. G. Bieker, M. Winter, and P. Bieker, Phys. Chem. Phys., 17, 8670 (2015).
- 4. J. Newman and K. E. Thomas-Alyea, Electrochemical Systems (John Wiley and Sons, Inc, Hoboken, New Jersey) 3rd ed. (2004).
- 5. A. C. West and J. S. Newman, in Modern Aspects of Electrochemistry, ed. B. E. Conway, J. O. '. M. Bockris, and R. E. White (Plenum Press, New York) Vol. 23, p. 113 (1992).
- 6. G. Prentice, Electrochemical Engineering Principles (Prentice Hall, Englewood Cliffs, NJ) p. 195 (1986).
- 7. V. R. Subramanian and R. E. White, J. Electrochem. Soc., 147, 1636 (2000).
- 8. I. Babuška, R. B. Kellogg, and J. Pitkäranta, Numer. Math., 33, 447 (1979).
- 9. H. F. Moulton, *Proc. of the London Math. Soc.*, **2**, 104 (1905). 10. M. Z. Bazant and D. Crowdy, "Conformal mapping methods for interfacial dynamics." Handbook of Materials Modeling, ed. S. Yip (Springer, Berlin) Vol. I, Art. 4.10 (2005).
- 11. W. F. Mitchell, Appl. Math. Comput., 220, 350 (2013).
- 12. M. Z. Bazant, K. Thornton, and A. Ajdari, Phys. Rev. E, 70, 24 (2004).
- 13. A. Subramaniam, J. Chen, T. Jang, N. R. Geise, R. M. Kasse, M. F. Toney, and V. R. Subramanian, J. Electrochem. Soc., 166, A3806 (2019).

- 14. A. Bonnefont, F. Argoul, and M. Z. Bazant, J. Electroanal. Chem., 500, 52 (2001)
- 15. R. Alkire, T. Bergh, and R. L. Sani, J. Electrochem. Soc., 125, 1981 (1978).
- 16. G. Caginalp, Arch. Ration. Mech. Anal., 92, 205 (1986).
- 17. S. Chen, B. Merriman, S. Osher, and P. Smereka, J. Comput. Phys., 135, 8 (1997).
- 18. S. Popinet and S. Zaleski, Int. J. Numer. Methods Fluids, 30, 775 (1999).
- 19. G. B. Less, J. H. Seo, S. Han, A. M. Sastry, J. Zausch, A. Latz, S. Schmidt, C. Wieser, D. Kehrwald, and S. Fell, J. Electrochem. Soc., 159, A697 (2012). 20. B. L. Trembacki, A. N. Mistry, D. R. Noble, M. E. Ferraro, P. P. Mukherjee, and
- S. A. Roberts, J. Electrochem. Soc., 165, E725 (2018).
- 21. Y. Zeng and M. Z. Bazant, SIAM J. Appl. Math., 74, 980 (2014).
- 22. Y. Zeng, P. Albertus, R. Klein, N. Chaturvedi, A. Kojic, M. Z. Bazant, and J. Christensen, J. Electrochem. Soc., 160, A1565 (2013).
- 23. A. Ferrese and J. Newman, J. Electrochem. Soc., 161, 1350 (2014).
- 24. C. Monroe and J. Newman, J. Electrochem. Soc., 152, A396 (2005)
- 25. V. Marra, COMSOL Blog, https://comsol.com/blogs/on-solvers-multigrid-methods/ last accessed: June 2020.
- 26. J. F. Grcar, Historia Mathematica, 38, 163 (2011).
- 27. L. H. Thomas, Watson Sci. Comput. Lab. Rept. (Columbia University, New York) 1 (1949).
- 28. Y. Saad, Iterative Methods for Sparse Linear Systems (SIAM, Philadelphia) 2nd ed. (2003).
- 29. W. E. Schiesser, The Numerical Method of Lines: Integration of Partial Differential Equations (Academic Press Inc, San Diego) (1991).
- 30. C. F. Curtiss and J. O. Hirschfelder, Proc. of the Nat. Academy of Sci. of the United States of America, 38, 235 (1952).
- 31. L. Petzold, SIAM J. on Scientific and Statistical Computing, 3, 367 (1982).
- 32. B. Gear, Scholarpedia, 2, 3162 (2007).
- 33. E. Hairer and G. Wanner, J. of Comp. and App. Math., 111, 93 (1982).
- 34. W. W. Hager, SIAM J. Numer. Anal., 13, 449 (1976).
- 35. L. H. Olesen, M. Z. Bazant, and H. Bruus, Phys. Rev. E, 82, 1 (2010).
- 36. V. Ramadesigan, P. W. C. Northrop, S. De, S. Santhanagopalan, R. D. Braatz, and V. R. Subramanian, J. Electrochem. Soc., 159, R31 (2012).
- 37. S. Kolluri, S. V. Aduru, M. Pathak, R. D. Braatz, and V. R. Subramanian, J. Electrochem. Soc., 167, 063505 (2020).
- 38. J. Liu, G. Li, and H. K. Fathy, IEEE Trans. Control Syst. Technol., 25, 1882 (2017).
- 39. M. Torchio, N. A. Wolff, D. M. Raimondo, L. Magni, U. Krewer, R. B. Gopaluni, J. A. Paulson, and R. D. Braatz, Proc. Am. Control Conf., 4536 (2015).
- 40. M. Torchio, L. Magni, R. D. Braatz, and D. M. Raimondo, J. Electrochem. Soc., 164, A949 (2017).
- 41. H. E. Perez, S. Dey, X. Hu, and S. J. Moura, J. Electrochem. Soc., 164, A1679 (2017).
- 42. A. Hoke, A. Brissette, D. Maksimović, A. Pratt, and K. Smith, IEEE Veh. Power and Propuls. Conf., 1 (2011).
- 43. C. Speltino, D. D. Domenico, G. Fiengo, and A. Stefanopoulou, Proc. IEEE Conf. Decis. Control, 3276 (2009).
- 44. M. Doyle, T. F. Fuller, and J. Newman, J. Electrochem. Soc., 140, 1526 (1993).
- 45. C. Y. Wang, W. B. Gu, and B. Y. Liaw, J. Electrochem. Soc., 145, 3407 (1998).
- 46. C. Y. Wang and V. Srinivasan, J. Power Sources, 110, 364 (2002).
- 47. V. R. Subramanian, D. Tapriyal, and R. E. White, *Electrochem. Solid-State Lett.*, 7, A259 (2004).
- 48. S. Santhanagopalan, Q. Guo, P. Ramadass, and R. E. White, J. Power Sources, 156, 620 (2006).
- 49. K. A. Smith, C. D. Rahn, and C. Y. Wang, J. Dyn. Syst. Meas. Control. Trans. ASME, 130, 011012 (2008).
- L. Cai and R. E. White, *J. Electrochem. Soc.*, **156**, A154 (2009).
   V. R. Subramanian, V. Boovaragavan, V. Ramadesigan, and M. Arabandi, J. Electrochem. Soc., 156, A260 (2009).
- 52. P. W. C. Northrop, V. Ramadesigan, S. De, and V. R. Subramanian, J. Electrochem. Soc., 158, A1461 (2011).
- 53. W. Fang, O. J. Kwon, and C. Y. Wang, Int. J. Energy Res., 34, 107 (2010).
- 54. Y. Ye, Y. Shi, N. Cai, J. Lee, and X. He, J. Power Sources, 199, 227 (2012).